Supplementary Materials for

High-valent iron-driven sulfamethoxazole removal during sludge dewatering process

Jialin Liang [a, *], Chengjian Li [a], Jiaqi Zhang [a], Liang Zhang [b, *], Jiewen Yang [a], Shuiyu Sun [d], Jonathan W.C. Wong [c]

a Guangdong Provincial Key Laboratory Lingnan Specialty Food Science and Technology, College of Resources and Environment, Zhongkai University of Agriculture and Engineering, Guangzhou, 510225, China

b Guangdong Provincial Key Laboratory of Environmental Pollution Control and Remediation Technology, School of Environmental Science and Engineering, Sun Yat-sen University, Guangzhou, 510275, China

c Research Center for Eco-Environmental Engineering, Dongguan University of Technology, Dongguan, Guangdong 523808, China

d School of Environmental Science and Engineering, Guangdong University of Technology, Guangzhou 510006, China

*Corresponding Author: Dr. Liang Zhang and Dr. Jialin Liang

E-mail: zhangliang25@mail.sysu.edu.cn (L. Zhang) and jialin.liang@zhku.edu.cn (J. Liang)

Number of Pages: 17

Number of Texts: 5

Number of Tables: 10

Number of Figures: 5

Content of this file:

Text S1 – UPLC-Q-Orbitrap HRMS for analyzing degradation products of SMX.

The used LC-MS/MS system was a Thermo Scientific Ultimate 3000 liquid phase system equipped with Q Exactive Orbitrap and an electrospray ionization source. A volume of 5 μL sample was injected to a Hypersil Gold C18 column (100 × 2.1 mm, 1.9 μm, Thermo Scientific, US) at 40 ℃. The LC flow was set to 300 μL/min using H_2O with 0.1% formic acid (A) and methanol (B) as eluents. The gradient program was performed as follows: 0-2 min, 98-80%A and 2-20% B; 2-16 min, 80-5% A and 20-95% B; 16-20 min, 5-98% A and 95-2% B.

Both positive and negative electrospray ionization were employed to obtain MS signals of analytes with spray voltages of +4.0 kV and -3.0 kV, respectively. The sheath gas flow rate, aux gas flow rate, and sweep gas flow rate were set to 35, 10, and 0 (arbitrary units), respectively. Capillary temperature and aux gas heater temperature were set to 320 °C and 350 °C, respectively. The instrument would automatically switch the positive and negative ion scanning mode and the scan mode was chosen as full MS scan-dd MS^2 and acquire first MS signals at 70000 FWHM and targeted MS/MS scan was set at a resolution of 17500 FWHM with a isolation width of 0.4 m/z. Meanwhile, the scan range of m/z was 50-750.

Text S2 – Quenching tests.

Quenching tests were conducted to assess the specific roles of •OH, $O_2^{\bullet-}$, $^1O_2$, and Fe(IV) in the SMX removal during the scrap iron + SPC conditioning process. To identify the contributions of •OH, $O_2^{\bullet-}$, $^1O_2$, and Fe(IV) on the SMX removal, radical scavenging tests were carried out using tert-butanol (TBA), P-benzoquinone (*p*-BQ), furfuryl alcohol (FFA), and methyl phenyl sulfoxide (PMSO) as quenchers for •OH, $O_2^{\bullet-}$, $^1O_2$, and Fe(IV) (Lei et al., 2023; Zhou et al., 2023). Nine experimental groups were established, including TBA, *p*-BQ, FFA, PMSO, scrap iron + SPC, scrap iron + SPC + TBA, scrap iron + SPC + *p*-BQ, scrap iron + SPC + FFA, scrap iron + SPC + PMSO. Under optimal conditions, the scrap iron + SPC system was evaluated in triplicate, and the contributions of •OH, $O_2^{\bullet-}$, $^1O_2$, and Fe(IV) to SMX removal were calculated using **Eqs. S1-S4**.

$$\text{Contribution of •OH (\%)} = \frac{C_e - (C_f - C_a)}{C_e} \times 100\% \quad (1)$$

$$\text{Contribution of } O_2^{\bullet-} \text{ (\%)} = \frac{C_e - (C_g - C_b)}{C_e} \times 100\% \quad (2)$$

$$\text{Contribution of } ^1O_2 \text{ (\%)} = \frac{C_e - (C_h - C_c)}{C_e} \times 100\% \quad (3)$$

$$\text{Contribution of Fe(IV) (\%)} = \frac{C_e - (C_i - C_d)}{C_e} \times 100\% \quad (4)$$

Where C_a, C_b, C_c, C_d, C_e, C_f, C_g, and C_i represents the SMX removal of the sludge after treatments by TBA, *p*-BQ, FFA, PMSO, scrap iron + SPC, scrap iron + SPC + TBA, scrap iron + SPC + *p*-BQ, scrap iron + SPC + FFA, and scrap iron + SPC + PMSO respectively.

Text S3 – Protocols of characterization methods for interaction between EPS and SMX.

The fluorescent components of the mixture of EPS and SMX were determined using EEM fluorescence spectroscopy (F-4600, Hitachi, Tokyo, Japan), per a protocol of (Chen et al., 2003). The fluorescence intensity linked to the mixture of EPS and SMX within each EEM could be derived through Parallel factor analysis (PARAFAC, EEMs-toolkit GUl 1.42) (Guillossou et al., 2021). In the PARAFAC test, each sample was repeated 20 times. The functional groups related to binding SMX in the EPS were identified through FTIR spectroscopy (Nicolet 6700, Thermo Fisher Scientific, Massachusetts, US). To further analyze the secondary structures of EPS proteins, the amide I region of EPS was analyzed using Peakfit software (Version 4.04, Software Inc., US). The surface chemical properties responsible for binding SMX in the EPS were analyzed using XPS (K-Alpha, Thermo Scientific, Massachusetts, US). Viscoelastic acoustic behaviors between the EPS and SMX were determined using QCM-D (Q-Sense E4, Göteborg, Sweden) under a protocol of Wu et al. (2022). The molecular compositions and fingerprints of dissolved organic components in the interaction between EPS and SMX were determined using the FT-ICR MS (7T SolariX, Bruker, Berlin, Germany) based on the methods reported in Huber et al. (2011).

Text S4 – Molecular docking and molecular dynamics simulation.

(i) Molecular docking

The Se-Met Methylmalonyl-CoA Epimerase was molecularly docked with sulfamethoxazole (SMX) using AutoDockTools-1.5.6 software. The three-dimensional structure of the protein was acquired from the Protein Data Bank (PDB, https://www.rcsb.org/). The structure of SMX was obtained from the ZINC database (http://zinc20.docking.org/) followed by hydrogenation and energy optimization using Avogadro software. A blind docking approach was employed to establish a grid box capable of including the whole protein for docking, and subsequently, the Lamarckian genetic algorithm was used for fifty iterations of docking (Devarajan et al., 2020).

(ii) Molecular dynamics simulation

Molecular dynamics simulations of the Se-Met Methylmalonyl-CoA Epimerase with SMX were conducted using the amber99sb force field in GROMACS 2020 (Van Der Spoel et al., 2005). The SMX was parameterized with the GAFF force field, and RESP electric potentials were computed using ORCA (Neese, 2018) and Multiwfn (Lu and Chen, 2012). The simulation system was employed using the TIP3P water model within a simulation box defined by periodic boundary conditions. The motion equations were integrated using a leap-frog algorithm with a time step of 2 fs. The LINUX algorithm was utilized to constrain hydrogen bond lengths, with parameters set to lincs_iter = 1 and lincs_order = 4. Simulations were performed under conditions of 300 K temperature and 1 bar pressure, with a time increment of 2 fs and a total simulation time of 100 ns (Hess et al., 2008). Post-simulation, trajectory analysis was conducted using the software's inherent tools to calculate the Root Mean Square Deviation (RMSD), Radius of Gyration (Rg), and hydrogen bonds. The most stable conformation was analyzed using PyMOL and Ligplot (Gao et al., 2021).

Text S5 – Sludge continuous conditioning reactor.

As modified by the previously used cycle instrument (Fan et al., 2023; Liang et al., 2020; Li et al., 2024), the sludge continuous conditioning reactor utilizing scrap iron and SPC was constructed to assess its effectiveness and operational stability in improving sludge dewatering and SMX removal. This system included a sludge conditioning tank, an *in-situ* generation of Fe tank, and a diluted H_2SO_4 tank. The *in-situ* generation of Fe tank comprised a mechanical stirrer, a heating plate, a thermometer, and a pH meter (PHS-3C, Leici, China). The experimental system generated an iron solution *in-situ* by reacting 100 g of scrap iron with 1.0 L of 0.1 M H_2SO_4 at 45 °C. For each cycle, 1.0 L sludge samples with SMX concentration of 150 mg/kg TS were conditioned by sequentially adding the iron solution (~2.0 mL/g TS), adjusting the pH to ~3.0 with 0.1 M H_2SO_4, and introducing SPC (22.5 mg/g TS). Following a 30-min Fenton-like reaction at 300 rpm, the mixture was dewatered in a high filter press for water content analysis, with residual scrap iron retained for reuse. The SMX concentration in the aqueous phase and solid phase was subsequently determined.

Table S1 – Batch tests design of different sludge conditioning procedures.

Batch test No.	Sludge treatments	Conditioning procedures
1	Fe^{2+} + PDS	Initial pH = 6.7 → 23.5 mg Fe^{2+}/g TS (1 min, 150 rpm) → 100.0 mg PDS/g TS (29 min, 150 rpm)
2	Fe^{2+} + CaO_2	Initial pH = 3.0 → 35.0 mg Fe^{2+}/g TS (1 min, 150 rpm) → 50.0 mg CaO_2/g TS (29 min, 150 rpm)
3	Fe^{2+} + SPC	Initial pH = 3.0 → 20.0 mg Fe^{2+}/g TS (1 min, 150 rpm) → 50.0 mg SPC/g TS (29 min, 150 rpm)
4	Scrap iron + SPC	Initial pH = 3.0 → 100.0 mg scrap iron/g TS (1 min, 150 rpm) → 20.0 mg SPC/g TS (29 min, 150 rpm)

Table S2 – Code and level of factors chosen for the trials.

Factors	Symbol	Level		
		-1.00	0.00	1.00
Scrap iron dosage (mg/g TS)	X_1	80.0	100.0	120.0
SPC dosage (mg/g TS)	X_2	17.5	20.0	22.5

Table S3 – Criteria of the response set for the optimization.

Response	Symbol	Goal	Lower Limit	Upper Limit
Water content of sludge cake (%)	Y_1	Minimize	52.0	56.0
SMX removal efficiency (%)	Y_2	Maximize	30.0	50.0

Table S4 – Design and response values.

No.	Scrap iron dosage (mg/g TS)	SPC dosage (mg/g TS)	Water content of sludge cake (%)	SMX removal efficiency (%)
	X_1	X_2	Y_1	Y_2
1	80	17.5	54.9	26.0
2	120	17.5	56.2	27.4
3	80	22.5	53.7	35.3
4	120	22.5	52.2	42.8
5	71.7	20	55.9	26.1
6	128.3	20	56.3	32.6
7	100	16.5	54.6	35.2
8	100	23.5	52.8	50.2
9	100	20	53.6	37.9
10	100	20	53.8	38.1
11	100	20	53.4	38.7
12	100	20	53.4	39.5
13	100	20	53.8	38.6

Table S5 – ANOVA for response surface quadratic model of water content of sludge cake.

Source	Sum of Squares	df	Mean Square	F-value	*p*-value
Model	18.53	5	3.71	13.15	0.019
A-Scrap iron	0.0095	1	0.0095	0.0335	0.8599
B-SPC	7.65	1	7.65	27.13	0.0012
AB	1.82	1	1.82	6.47	0.0385
A^2	8.58	1	8.58	30.44	0.0009
B^2	0.0871	1	0.0871	0.3089	0.5957
Residual	1.97	7			
Lack of Fit	1.81	3	0.6039	14.95	0.0122
Pure Error	0.1616	4	0.0404		
Cor Total	20.50	12			

Table S6 – ANOVA for response surface quadratic model of SMX removal efficiency.

Source	Sum of Squares	df	Mean Square	F-value	*p*-value
Model	544.77	5	108.95	32.99	0.0001
A-Scrap iron	41.06	1	41.06	12.43	0.0097
B-SPC	264.22	1	264.22	79.99	< 0.0001
AB	9.55	1	9.55	2.89	0.1329
A^2	202.02	1	202.02	61.16	0.0001
B^2	11.46	1	11.46	3.47	0.1048
Residual	23.12	7	3.30		
Lack of Fit	21.57	3	7.19	18.55	0.0082
Pure Error	1.55	4	0.3876		
Cor Total	567.89	12			

Table S7 – Band assignments for the protein secondary structures of the mixture of EPS and SMX before and after scrap iron + SPC treatment.

Samples	Protein secondary structures					
	Aggregated strands (1610-1625 cm^{-1})	β-Sheet (1630-1640 cm^{-1})	Random coil (1640-1645 cm^{-1})	α-Helix (1648-1657 cm^{-1})	3-Turn helix (1659-1672 cm^{-1})	Antiparallel β-sheet/aggregated strands (1680-1695 cm^{-1})
EPS	8.7%	21.3%	10.5%	19.9%	24.3%	15.1%
EPS + SMX	8.2%	20.4%	13.9%	19.2%	23.3%	14.9%
EPS after scrap iron + SPC treatment	10.1%	24.9%	10.1%	15.5%	24.8%	14.6%
EPS + SMX after scrap iron + SPC treatment	19.1%	25.6%	10.4%	14.4%	22.2%	8.3%

Table S8 – Molecular composition of the EPS + SMX before and after scrap iron + SPC treatment.

Samples	Carbohydrates (%)	Protein/Aliphatic (%)	Lipids (%)	Tannins (%)	Lignin (%)	Unsaturated hydrocarbons (%)	Condensed aromatic structures (%)
EPS	0.79	1.79	21.1	2.49	16.8	0.86	23.8
EPS + SMX	1.56	5.56	25.0	2.31	20.7	0.79	17.6
EPS after scrap iron + SPC treatment	1.42	7.01	28.2	2.28	22.1	0.74	14.2
EPS + SMX after scrap iron + SPC treatment	1.45	7.36	30.4	2.22	22.3	0.07	12.9

Table S9 – SMX intermediates after scrap iron + SPC treatment.

Product ID	Molecular formula	Observed m/z ([M+H]+)	Calculated m/z ([M+H]+)	Proposed structure
SMX	$C_{10}H_{11}N_3O_3S$	254.05939	254.05931	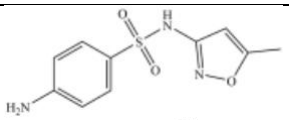
P1	$C_{10}H_{11}N_3O_4S$	270.0543	270.05402	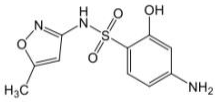
P2	$C_{10}H_{10}N_2O_3S$	239.04849	239.04846	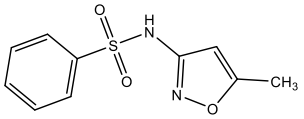
P3	$C_{10}H_{10}N_2O_4S$	255.04340	255.04312	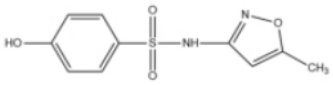
P4	$C_{10}H_{16}N_2O_5S$	277.08527	277.08466	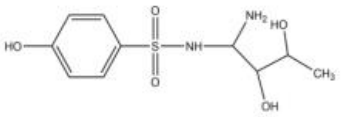
P5	C_6H_7NO	110.06004	110.06005	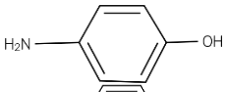
P6	$C_6H_5NO_3$	140.03422	140.03421	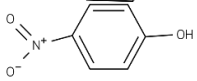
P7	C_6H_6O	95.04914	95.04915	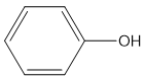
P8	$C_6H_7NO_2S$	158.02703	158.02702	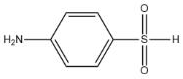
P9	$C_6H_5NO_2S$	156.01138	156.01065	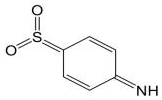
P10	C_6H_5NO	108.04439	108.04439	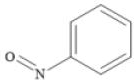
P11	$C_6H_5NO_2$	124.03931	124.03929	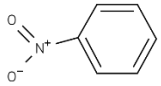
P12	$C_4H_4N_2O_2$	113.03455	113.03448	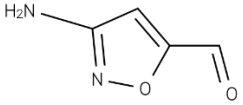

Table S10 – Chemical cost of different sludge conditioning methods.

Sludge conditioning methods	Chemical reagents	Unit price (USD/ton)	Dosages (kg/ton TS)	Total chemical cost (USD/ton TS)	Reference
Fe^{2+} + PMS	Fe^{2+} PMS	64.7 600.0	900.0 418.0	309.0	Xiao et al. (2022)
Chalcopyrite + SPC	H_2SO_4 Chalcopyrite SPC	78.0 800.0 283.9	10.0 200.0 12.5	164.3	Liang et al. (2024)
$CoFe_2O_4$ + PMS	$CoFe_2O_4$ PMS	1000.0 600.0	80.0 60.0	116.0	Sang et al. (2024)
BC-800 + Fe^{2+} + PMS	H_2SO_4 Biochar Fe^{2+} PMS NaOH	78.0 300.0 64.7 600.0 500.0	10.0 120.0 25.0 100.0 10.0	103.4	Wang et al. (2025)
Scrap iron + SPC	H_2SO_4 Scrap iron SPC	78.0 116.0 283.9	10.0 107.1 22.5	19.6	This study

Note: Unit price of chemicals was determined according to http://www.alibaba.com/.

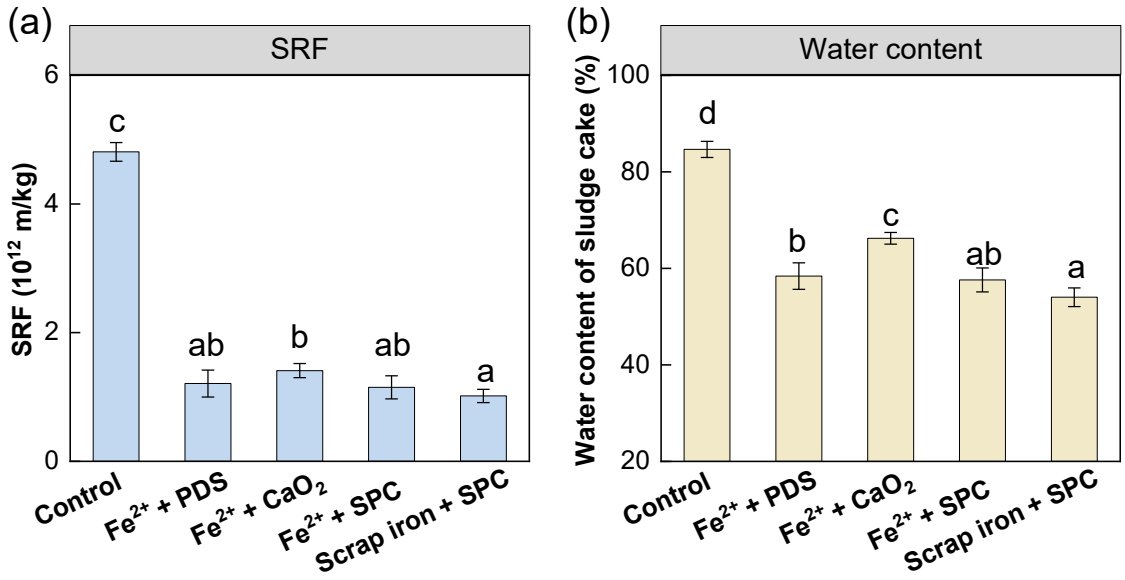

Fig. S1 – SRF values (a) and Water content of sludge cake (b) of different sludge treatments (Fe^{2+} + PDS: Initial pH = 6.7, Fe^{2+} dosages = 23.5 mg/g TS, PDS dosage = 100.0 mg /g TS; Fe^{2+} + CaO_2: Initial pH = 3.0, Fe^{2+} dosages = 35.0 mg/g TS, CaO_2 dosage = 50.0 mg /g TS; Fe^{2+} + SPC: Initial pH = 3.0, Fe^{2+} dosages = 20.0 mg/g TS, SPC dosage = 50.0 mg /g TS; Scrap iron + SPC: Initial pH = 3.0, Scrap iron dosage = 100 mg/g TS, SPC dosage = 20 mg/g TS; Significant differences ($p < 0.05$) among the various groups are indicated using lowercase characters).

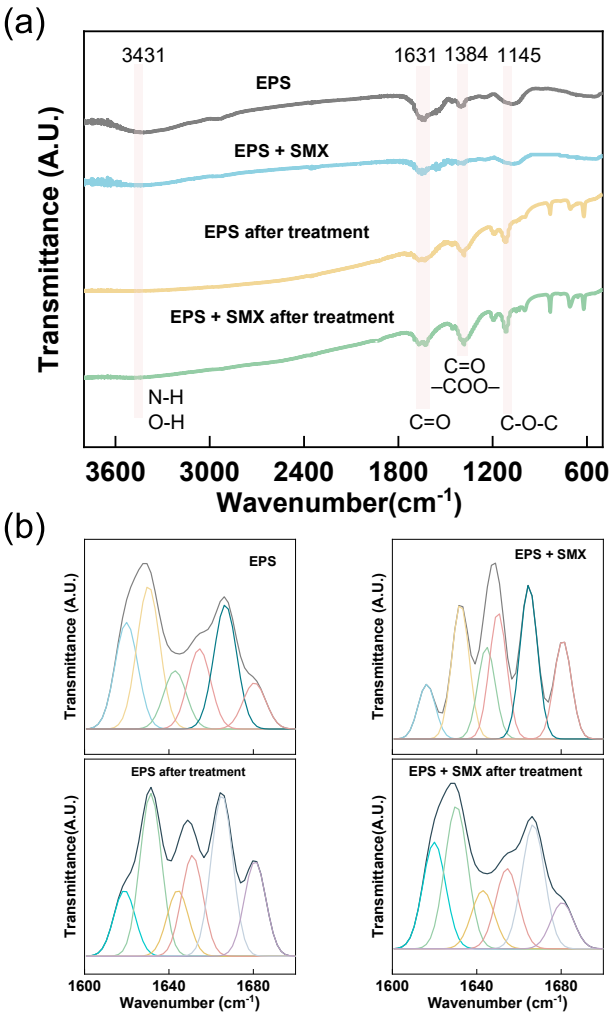

Fig. S2 – (a) FTIR spectra and (b) protein secondary structures of the EPS + SMX before and after treatment (TOC concentration of EPS = 85.2 ± 0.2 mg/L, SMX concentration = 3.0 mg/L, temperature = ~25 °C, scrap iron dosage = 107.1 mg/g TS, SPC dosage = 22.5 mg/g TS, initial pH = 3.0, and reaction time = 30 min).

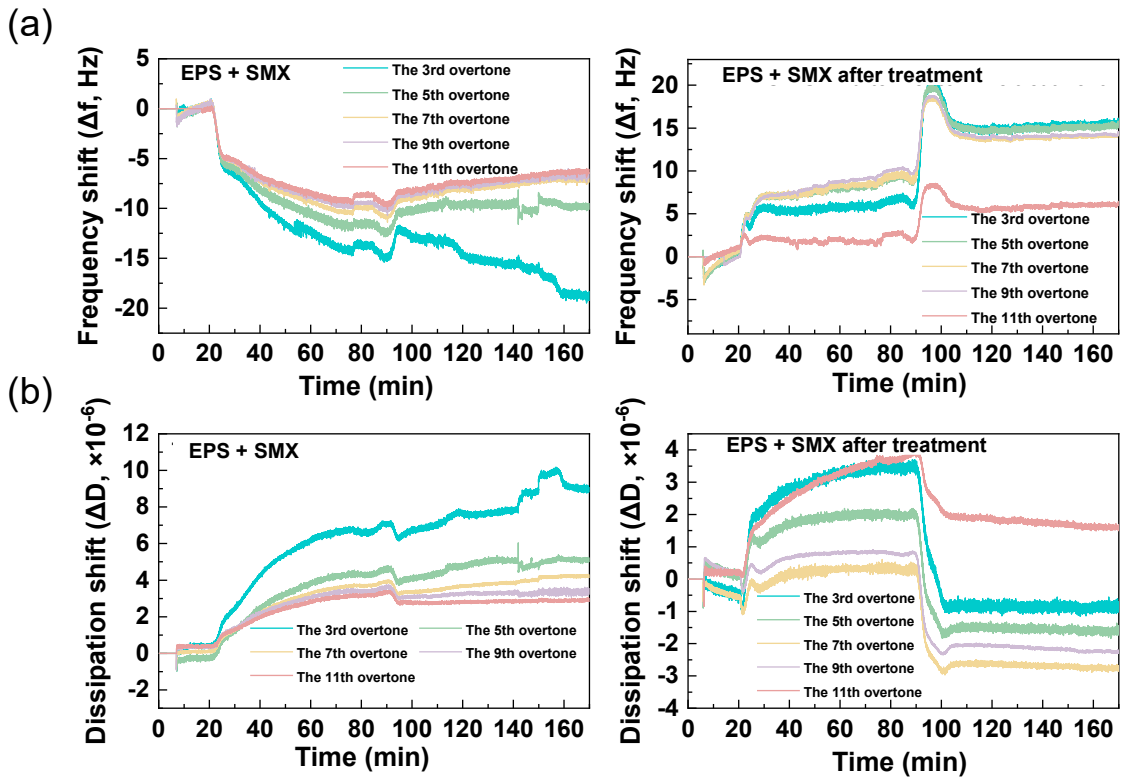

Fig. S3 – Viscoelastic acoustic behaviors between the EPS + SMX before and after treatment by QCM-D: (a) Δf and (b) ΔD (TOC concentration of EPS = 85.2 ± 0.2 mg/L, SMX concentration = 3.0 mg/L, temperature = ~25 °C, scrap iron dosage = 107.1 mg/g TS, SPC dosage = 22.5 mg/g TS, initial pH = 3.0, and reaction time = 30 min).

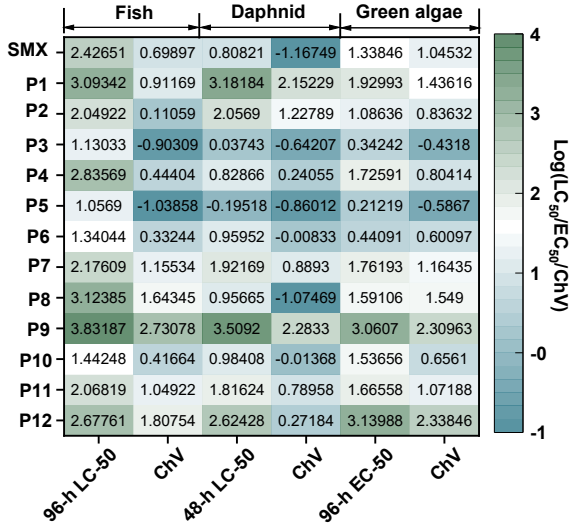

Fig. S4 – The potential toxicity of SMX degradation products after the scrap iron + SPC treatment.

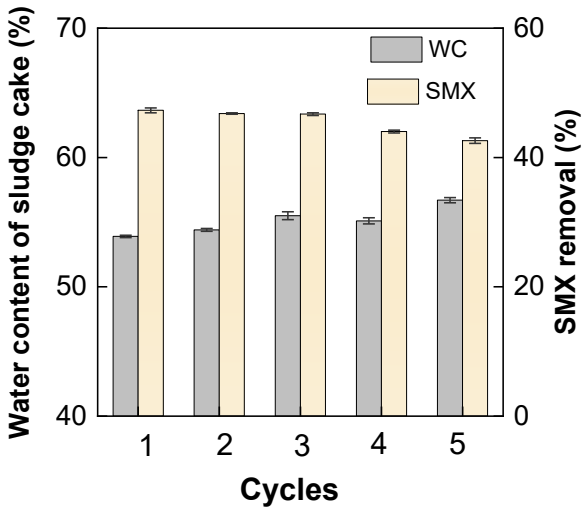

Fig. S5 – Results of cycle tests with the scrap iron + SPC treatment.

References

Chen W, Westerhoff P, Leenheer JA, Booksh K (2003). Fluorescence excitation-emission matrix regional integration to quantify spectra for dissolved organic matter. Environmental Science & Technology, 37(24): 5701-5710.

Devarajan D, Liang L, Gu B, Brooks SC, Parks JM, Smith JC (2020). Molecular dynamics simulation of the structures, dynamics, and aggregation of dissolved organic matter. Environmental Science & Technology, 54(21): 13527-13537.

Fan X, Wang Y, Zhang D, Zhang S, Liu C, Liu M (2023). Comprehensive assessment of sludge conditioning using pyrite acid eluent-activated peroxymonosulfate: evaluation of dewaterability, heavy metal risk, and ore recovery. Waste Management, 170: 82–92.

Gao Q, Bie P, Tong X, Zhang B, Fu X, Huang Q (2021). Complexation between high-amylose starch and binary aroma compounds of decanal and thymol: Cooperativity or competition? Journal of Agricultural and Food Chemistry, 69(39): 11665-11675.

Guillossou R, Le Roux J, Goffin A, Mailler R, Varrault G, Vulliet E, Morlay C, Nauleau F, Guerin S, Rocher V, Gasperi J (2021). Fluorescence excitation/emission matrices as a tool to monitor the removal of organic micropollutants from wastewater effluents by adsorption onto activated carbon. Water Research, 190: 116749.

Hess B, Kutzner C, Van Der Spoel D, Lindahl E (2008). GROMACS 4: algorithms for highly efficient, load-balanced, and scalable molecular simulation. Journal of Chemical Theory and Computation, 4(3): 435-447.

Huber SA, Balz A, Abert M, Pronk W (2011). Characterisation of aquatic humic and non-humic matter with size-exclusion chromatography – organic carbon detection – organic nitrogen detection (LC-OCD-OND). Water Research, 45(2): 879-885.

Li C, Zhang Y, Ren J, Mo Z, Liang J, Ye M, Ou W, Sun S, Zhu S (2024). In-situ generation of iron activated percarbonate for sustainable sludge dewatering. Science of the Total Environment, 922: 171235.

Lei Q, Liu M, Yang T, Chen M, Qian L, Mao S, Cai J, Zhao H (2023). Controllable generation of sulfate and hydroxyl radicals to efficiently degrade perfluorooctanoic acid in cathode-dominated electrochemical process. ACS ES&T Water, 3(11): 3696-3707.

Liang J, Huang J, Zhang L, Sun F, Ye M, Liao X, Huang S, Sun S (2020). Enhanced dewaterability of high-level waste activated sludge through a Fenton-like process employing pretreated zero valent scrap iron as an in-situ cycling iron source. Journal of Hazardous Materials, 391: 122219.

Liang J, Zhang L, Li C, Mo Z, Ye M, Zhu Z, Sun S, Wong JW (2024). Triclocarban transformation and removal in sludge conditioning using chalcopyrite-triggered percarbonate treatment. Journal of Hazardous Materials, 463: 132944.

Lu T, Chen F (2012). Multiwfn: A multifunctional wavefunction analyzer. Journal of Computational Chemistry, 33(5): 580-592.

Neese F (2018). Software update: the ORCA program system, version 4.0. WIREs Computational Molecular Science, 8(1): e1327.

Sang W, Deng M, Pang L, Cheng K, Li M, Gan F, Zhang Q, Zhang S (2024). Insights into the effects of cobalt ferrite nanoparticles activated peroxymonosulfate on waste activated sludge dewaterability during ciprofloxacin degradation. Journal of Environmental Chemical Engineering, 12(4): 113163.

Van Der Spoel D, Lindahl E, Hess B, Groenhof G, Mark AE, Berendsen HJ (2005). GROMACS: fast, flexible, and free. Journal of Computational Chemistry, 26(16): 1701-1718.

Wang S, Luo F, He L, Liu Z, Wang J, Liao Z, Hou H, Li J, Ning X, Chen Z (2025). Enhanced sludge dewaterability and confined antibiotics degradation in biochar-mediated chemical conditioning through modulating Fe oxidative states distribution and reaction sites in multiphase. Water Research, 270: 122789.

Wu B, Wang H, Li W, Dai X, Chai X (2022). Influential mechanism of water occurrence states of waste-activated sludge: Potential linkage between water-holding capacity and molecular compositions of EPS. Water Research, 213: 118169.

Xiao K, Abbt-Braun G, Borowska E, Thomagkini X, Horn H (2022). Solid–liquid distribution of ciprofloxacin during sludge dewatering after Fe (II)-activated peroxymonosulfate treatment: focusing on the role of dissolved organic components. ACS ES&T Engineering, 2(5): 863-873.

Zhou Y, Yang S, Wang M, Guan Y, Ma J (2023). Fast degradation of atrazine by nZVI-Cu0/PMS: Re-evaluation and quantification of reactive species, generation pathways, and application feasibility. Water Research, 243: 120311.